DOI: 10.1113/EP087545

Electroporated GLUT4-7*myc*-GFP detects *in vivo* glucose transporter 4 translocation in skeletal muscle without discernible changes in GFP-patterns

Jonas Roland Knudsen[1], *Carlos Henriquez-Olguin*[1], *Zhencheng Li*[1], *Thomas Elbenhardt Jensen*[1,2]

[1]*Section of Molecular Physiology, Department of Nutrition, Exercise and Sports, University of Copenhagen, Denmark.*

[2]*Correspondence: Thomas Elbenhardt Jensen, Section of Molecular Physiology, Department of Nutrition Exercise and Sports, University of Copenhagen, Universitetsparken 13, 2100, Copenhagen, Denmark.*

tejensen@nexs.ku.dk

Running title: An easy way to assess exercise-stimulated GLUT4 translocation

Keywords: skeletal muscle, exercise, glucose transport

Word counting: 4882

Number of references: 61

Primary subject area: Muscle

Secondary subject: Human, Environmental & Exercise

What is the central question of this study?

Resolving the mechanism(s) leading to glucose transporter 4 (GLUT4) translocation to the muscle surface membrane has great therapeutic potential. However, the measurement of GLUT4 translocation is technically challenging. Here, we asked whether electroporation of GLUT4-7*myc*-GFP into skeletal muscle could be used as a tool to study GLUT4 translocation *in vivo*.

What is the main finding and its importance?

By acutely inducing GLUT4-7*myc*-GFP expression in skeletal muscle, we verified that *in vivo* exercise and AICAR stimulation increased the GLUT4 presence in the sarcolemma measured as *myc*-signal. Importantly, the increased *myc*-signal in the sarcolemma was not accompanied by major visual changes in the distribution of the GFP signal.

Abstract:

Insulin and exercise lead to translocation of the glucose transporter 4 (GLUT4) to the surface membrane of skeletal muscle fibres. This process is pivotal for facilitating glucose uptake into skeletal muscle. To study this, a robust assay to directly measure the translocation of GLUT4 in adult skeletal muscle is needed. Here, we aimed to validate a simple GLUT4 translocation assay using a genetically encoded biosensor in mouse skeletal muscle. We transfected GLUT4-7*myc*-GFP into mouse muscle to study live GLUT4 movement and to evaluate GLUT4 insertion in the muscle surface membrane following *in vivo* running exercise and pharmacological activation of AMP activated protein kinase (AMPK). Transfection led to expression of GLUT4-7*myc*-GFP that were dynamic in live flexor digitorum brevis fibres and which, upon insulin stimulation, exposed the *myc*-epitope extracellularly. Running exercise, as well as AMPK-activation by 5-Aminoimidazole-4-carboxamide ribonucleotide, induced ~125% and ~100% increase in extracellularly exposure of GLUT4 in the surface membrane of tibialis anterior muscle. Interestingly, the clear increase in surface-exposed GLUT4 content by insulin, exercise or AMPK activation was not accompanied by any discernible reorganization of the GLUT4-GFP signal. In conclusion, we provide a detailed description of an easy to use translocation assay to study GLUT4 accumulation at the surface membrane by exercise and exercise-mimicking stimuli. Notably, our analyses revealed that increased GLUT4 surface membrane accumulation was not accompanied by a discernible change in the GLUT4 localization pattern.

Abbreviations:

AICAR – 5-Aminoimidazole-4-carboxamide ribonucleotide

AMPK – AMP activated protein kinase

FDB – Flexor digitorum brevis

GLUT4 – Glucose transporter 4

SOL – Soleus

TA – Tibialis anterior

Introduction:

Insulin resistance at the level of skeletal muscle is an early hallmark during the development of type 2 diabetes (DeFronzo & Tripathy, 2009; Warram, Martin, Krolewski, Soeldner, & Kahn, 1990). Interestingly, although insulin resistant and diabetic subjects exhibit decreased insulin-stimulated glucose handling in peripheral tissues, exercise-induced glucose uptake in muscle is preserved (Martin, Katz, & Wahren, 1995). This highlights the importance of understanding the molecular mechanisms regulating exercise induced glucose uptake, both from a clinical and a pharmaceutical point of view. Glucose transporter 4 (GLUT4) isoform is the main glucose transporter responsible for insulin- and contraction-induced glucose uptake (Zisman et al., 2000). Upon stimulation, GLUT4 content in the muscle fibre surface membrane increases, a process considered as the rate limiting step for glucose uptake during most contraction conditions (Richter & Hargreaves, 2013) as well as during insulin stimulation in type 2 diabetic subjects (Cline et al., 1999; Goodpaster et al., 2014; Shepherd & Kahn, 1999). Numerous studies of cultured muscle and fat cells have provided detailed insight into GLUT4 localization and trafficking (Jaldin-Fincati, Pavarotti, Frendo-Cumbo, Bilan, & Klip, 2017; Leto & Saltiel, 2012). Unfortunately, these undifferentiated cell types poorly recapitulate the complex architecture and function of fully adult skeletal muscle fibres (Deshmukh et al., 2015).

Previous studies performed *in vivo* imaging of GLUT4 in adult muscle and demonstrated that insulin and contraction translocated GLUT4 from a resting non-structured aggregate localization in small and larger vesicles enriched in the perinuclear and trans-Golgi network regions. This resulted in a distinct stimulated pattern with accumulation of GLUT4 in the sarcolemma and in transverse striations, presumably t-tubules (Lauritzen, Galbo, Brandauer, Goodyear, & Ploug, 2008; Lauritzen, Galbo, Toyoda, & Goodyear, 2010). Despite the value of these studies, the techniques applied are challenging, time-consuming and have never been applied in transgenic animals. This has limited the scientific progress in understanding exercise-induced muscle glucose transport in fully differentiated muscle tissue. To overcome

this disparity, there is a need for a simple but robust approach to measure GLUT4 translocation to the surface membrane of adult muscle fibres.

Ideally, such an approach should be easily applicable in transgenic animals to gain mechanistic insight into GLUT4 regulators. Several methods have previously been used to study GLUT4 translocation, including affinity labelling of exofacially exposed GLUT4 using bis-mannose photolabels (Hansen, Nolte, Chen, & Holloszy, 1998; Holman et al., 1990; Lund, Holman, Schmitz, & Pedersen, 1995), western blotting of GLUT4 content in giant sarcolemmal vesicles chemically released from the plasma membrane (Kristiansen, Hargreaves, & Richter, 1996; Ploug et al., 1993) and biochemical fractionation (Klip, Ramlal, Young, & Holloszy, 1987; Marette, Burdett, Douen, Vranic, & Klip, 1992; Rose, Jeppesen, Kiens, & Richter, 2009). However, large tissue demands and/or *ex vivo* labelling requirements make these approaches suboptimal for *in vivo* studies in small rodents. As *in vivo* alternatives, immunofluorescence co-staining of GLUT4 and a plasma membrane marker (Bradley et al., 2015; Sylow et al., 2016) as well as overexpression of GFP-conjugated GLUT4 (Lauritzen et al., 2010) have been performed. However, in practical terms laser scanning confocal microscopy can only resolve objects at least 200-350 nm apart (Schermelleh, Heintzmann, & Leonhardt, 2010). Therefore, these studies cannot distinguish between GLUT4 accumulation in subsarcolemmal regions and bona fide insertion of GLUT4 into the ~10 nm thick sarcolemmal membrane (Mauro & Adams, 1961). This is a drawback since insulin has been suggested primarily to affect fusion of vesicles already localized in close proximity to the surface membrane in skeletal muscle (Lizunov et al., 2012).

As a promising alternative, overexpression of GLUT4 with a *myc* or an HA epitope inserted into the exofacial loop between the first two hydrophobic transmembrane domains can be used for direct immunological determination of GLUT4 translocation to the surface membrane (Bogan, McKee, & Lodish, 2001; Kanai et al., 1993). This tool was used to generate transgenic mice expressing GLUT4*myc* in skeletal muscle (Schertzer et al., 2009). It is also compatible with acute overexpression by electroporation (Ueda et al., 2010), potentially allowing verification of GLUT4 membrane insertion in any transgenic model and/or intervention of choice. Here, we set up an approach to measure *in vivo* running-induced GLUT4 translocation. We showed insulin responsiveness and functionality of the

GLUT4-7*myc*-GFP construct in isolated live flexor digitorum brevis (FDB) muscle fibres and verified the utility of this construct as a robust GLUT4 translocation assay in the contexts of *in vivo* exercise and 5-Aminoimidazole-4-carboxamide ribonucleotide (AICAR)-stimulation. Notably, using GLUT4-7*myc*-GFP we demonstrated that increased GLUT4 translocation, measured as surface exposure of the *myc*-tag, was not accompanied by the previously described redistribution of GLUT4 GFP signal to a global striated pattern.

Methods:

Ethical approval

All animal experiments were approved by the Danish Animal Experimental Inspectorate (Ref# 2014-15-2934-01037) and complied with the European Union legislation as outlined by the European Directive 2010/63/EU. The investigators understand the ethical principles under which *Experimental Physiology* operates and the current work adheres to the standards outlined in the ARRIVE reporting guidelines.

pB-GLUT4-7*myc*-GFP gene transfer into mouse muscles

C57BL/6JRj female mice aged 10-16 weeks, were fed *ad libitum* with a standard rodent chow diet and exposed to a 12 h:12 h light-dark cycle. FDB or tibialis anterior (TA) muscles were electroporated *in vivo* according to a previously described protocol (DiFranco, Quinonez, Capote, & Vergara, 2009) with a few modifications. Briefly, mice were given a subcutaneous injection of Rimadyl (7.5 mg/kg) as analgesic and anaesthetized using 2-4% isoflurane. For FDB muscles, 10 µl of 0.36 mg/ml hyaluronidase (H3884, Sigma) was injected through the skin at the heel into the footpad. After one hour, 20 µl of 0.5 mg/ml pB-GLUT4-7*myc*-GFP plasmid (a gift from Jonathan Bogan, Addgene plasmid #52872) (Bogan et al., 2001) was injected into the same location. Six pulses of 20 ms were delivered at 1 Hz with the voltage amplitude adjusted to yield an electric field of approximately 75 V/cm using acupuncture needles (0.20 x 25 mm, Tai 135 Chi, Lhasa OMS) connected to an ECM 830 BTX electroporator (BTX Harvard Apparatus). For TA, the leg was shaved and hyaluronidase and plasmid were injected intramuscularly. The muscle was injected with 20 µl of 0.36 mg/ml hyaluronidase followed by 20 µl of 2 mg/ml pB-GLUT4-7*myc*-GFP plasmid or saline after one hour. The muscles then received 10 pulses of 20 ms duration delivered at 1 Hz using a BTX

caliper electrode (1x1 cm) adjusted to reach 100 V/cm (#45-0101 Caliper Electrode, BTX Caliper Electrodes, USA). After the procedure, the animals were transferred back to their cages and allowed to recover. The terminal experiment was performed 5-7 days after electroporation.

Fibre isolation and live imaging

The animals were anaesthetized (6 mg pentobarbital sodium and 0.25 mg lidocaine/100 g body weight) and euthanized by cervical dislocation. One hindlimb was removed and the thigh and toes were pinned on a Sylgard-coated petri dish containing enough Dulbecco's Phosphate-Buffered Saline (14190-094, Gibco) to submerge the hindlimb and placed under a dissection microscope. The paw was placed with the plantar side facing up and the skin was removed, exposing the underlying FDB muscle. The proximal tendon was cut and the FDB muscle was separated from its connective tissue using a spring-scissor by gently cutting from the heel towards the digits until the distal tendons were exposed. The tendons were cut and the excised FDB muscle was further cleaned from visible fat tissue and blood vessels. The same procedure was performed for the contralateral paw. The muscles were then incubated for 3 hours in DMEM (10567014, Gibco) containing 1.5 mg/ml collagenase type 1 from clostridium histolyticum (C0130, Sigma-Aldrich) and 1 mg/ml bovine serum albumin (9048-46-8, Sigma-Aldrich) at 37°C on a rotator. After the collagenase-treatment, individual fibres were released by repeatedly pipetting the muscle up into a 0.5 ml. glass pipette and down in 2 ml DMEM in a glass vial. The released fibres were transferred to a new glass vial using the glass pipette and the procedure was repeated 5-7 times for release of additional fibres. The glass vial was then incubated at 37 °C for 20 min to allow fibres to concentrate at the bottom. Excess media was removed and the remaining approximately 600 µl was then spread out in 50 µl aliquots on 35x14 mm glass bottom microwell dishes (P35G-1.5-14-C, MatTek Corporation) or coverslips in a 6 well plate, both coated with matrigel. After 2 hours, additional 2 ml of DMEM containing 5% fetal bovine serum (26140-087, Gibco) was added to the dish/well and the muscle fibres were then cultured overnight. The next day, muscle fibres were either used for live imaging or fixed in the presence or absence of insulin (60nM, 30 min) (Actrapid, Novo Nordisk A/S). One group of muscle fibres were incubated with wortmannin (500nM) (S2758, Selleckchem) for 30 min before and

during insulin stimulation. For fixation, muscle fibres were incubated in Zamboni fixative (AMPQ44816.1000, VWR) containing 4% paraformaldehyde for 20 min.

Running experiment

Mice were acclimatized to running treadmills twice before they were subjected to the gene transfer procedure. 3 days after the gene transfer procedure, the mice were acclimatized one last time to the treadmill. On day 4, the mice were subjected to a maximal running capacity test comprised of a ramp protocol with continuously increased running speed of 3 m/min similar to (Ayachi, Niel, Momken, Billat, & Mille-Hamard, 2016) at a 10° incline until exhaustion, determined either as contact with the shock grid two consecutive times within 5 seconds or by contact with the grid the 5th time. On day 7, the mice were fasted for 3 hours followed by either running at 75% of maximal running speed for 10 min and 5 min at 85% of maximal running speed or remained at rest in their cage for 15 min. Immediately post exercise/rest, the mice were euthanized and TA muscles were dissected out and fixated in Zamboni fixative for 4 hours to determine GLUT4 surface membrane accumulation. Soleus (SOL) muscles were also dissected and snap frozen in liquid nitrogen for cell signalling analysis. A subset of the mice were injected with [3H]2-DG (PerkinElmer) intraperitoneally prior to the running to measure *in vivo* 2-deoxyglucose (2-DG) uptake into the muscles, as described previously (Sylow et al., 2016). For *in vivo* insulin-stimulation, anaesthetized (6 mg pentobarbital sodium and 0.25 mg lidocaine/100 g body weight) mice received insulin (0.5 U/kg body weight) retro-orbitally 30 min prior to tissue collection. All mice were euthanized by cervical dislocation.

Intramuscular AICAR injections

In the morning, within 30 min after ended dark cycle, the mice were anaesthetized sequentially using 2% isoflurane as inhalation anaesthetic. Ten min into anaesthesia, the hind limbs of a given mouse were quickly shaved. The mouse received an intramuscular injection with 25 µl saline solution containing AICAR (9 mM) into TA in one leg and 25 µl saline in the contralateral TA using a 30 gauge insulin syringe (324826, BD Micro-Fine). We estimated TA muscle weight of these 14 weeks old mice to be ~ 50 mg. Assuming the density of mammalian muscle to be 1.06 g/ml (Close, 1972), injecting 25 µl of 9 mM AICAR should provide a final concentration of around 3 mM in the muscle if equally distributed.

This concentration is known to activate AMP activated kinase (AMPK) (Jensen et al., 2015). Mice were kept under anaesthesia for one hour and then euthanized by cervical dislocation before TA muscles were quickly removed and snap frozen in liquid nitrogen for determination of cell signalling. A sub-group of four mice were injected with GLUT4-7*myc*-GFP in both legs seven days prior to the terminal experiment. A piece of the TA muscle from these mice was immersed in Zamboni fixative for four hours to assess GLUT4 surface membrane accumulation.

Immunofluorescence preparation and Imaging

For live muscle fibre imaging cultured FDB fibres were kept in DMEM containing 5% fetal bovine serum and imaged by a microscope with integrated incubator at 37° C in 95% O2 and 5% CO2. The fixed cultured FDB fibres were washed 3x10 min in PBS and incubated in blocking buffer (1% bovine serum albumin, 5% goat serum (16210-064, Gibco), 0.1% Na Azide (247-852, Merck) for 30 min. The muscle fibres were then incubated with an antibody against the *myc*-tag (2272, CST) diluted 1:400 in blocking buffer for one hour. Then, the fibres were washed in PBS containing 0.04% saponin (w/v) (27534-187, VWR) for 3x10 min and incubated with an Alexa 568 secondary antibody (A10042, Life Technologies) diluted 1:400 in blocking buffer containing 0.04% saponin for 120 min. Finally, the fibres were washes 3x10 min in PBS and mounted on glass slides in Vectashield (H-1000, Vector Laboratories). Following fixation, TA muscles were transferred to a Sylgaard dish and isolated into smaller bundles using fine forceps. The bundles were transferred to a storage solution containing PBS and glycerol (1:1) and kept at 4° overnight. The next day, the bundles were teased apart into individual fibres and washed 3x 10 min in PBS before 30 min incubation in blocking buffer. The fibres were then incubated in blocking buffer containing *myc* antibody for one hour. As part of the antibody validation, a several fibres were incubated with *myc* antibody in blocking buffer containing 0.04% saponin to permeabilize the surface membrane. All fibres were then washed 3x10 min in PBS containing 0.04% saponin and incubated with Alexa 568 antibody in blocking buffer containing 0.04% saponin for 120 min. Finally, the muscle fibres were individually transferred to mounting media on a glass slide and covered by a coverslip. Imaging was performed using a 63x 1.4 NA Plan-Apochromat objective on a Zeiss 780 microscope driven by Zeiss Zen Black 2012.

Image Analysis

Protein tracking on the live-cell images was performed using the manual tracking plugin in ImageJ 1.51u 64-bit (National Institute of Health). For quantification of GLUT4 surface membrane accumulation, the images were analysed with a semi-automated approach using ImageJ. In short, the *myc* and GFP channels were duplicated and the new images underwent a background subtraction, a Gaussian blur adjustment (radius = 2), and were made binary. From these binary images, regions of positive GFP and *myc* signal were selected and overlaid onto the original images for quantification of integrated density of GFP and *myc* signal respectively. Images were exported in 8-bit TIF format, linearly adjusted, cropped and resized using ImageJ or Adobe Photoshop CC 2015.

Western blotting

Western blotting and sample preparation was performed as previously described (Madsen et al., 2018). In short, the muscles were homogenized in ice-cold lysis buffer (50 mM Tris base, 150 mM NaCl, 1mM EDTA, 1 mM EGTA, 50 mM sodium fluoride, 5 mM pyrophosphate, 2 mM sodium orthovanadate, 1 mM dithiothreitol, 1 mM benzamidine, 0.5% protease inhibitor cocktail (Sigma P8340), 20% NP-40, pH 7.4) for one min at 30 Hz using a tissue lyser (Qiagen). The homogenate was then rotated end over end for 30 min at 4 °C and subsequently centrifuged at 18,320 G for 20 min at 4 °C. The supernatant was transferred to new tubes and the protein concentration was measured using the bicinchonic acid method. To determine phosphorylation levels of proteins equal amounts of protein were subjected to electrophoresis on 5-12% self-cast SDS-PAGE gels and transferred by semidry blotting to polyvindylidenedifluoride membranes. Membranes were blocked for 15 min in Tris-buffered saline with 0.5 ‰ tween 20 and 3% skimmed milk powder at room temperature. Then overnight incubation at 4 °C with primary antibody was performed. Next day the membranes were washed in TBST and incubated with secondary horseradish peroxidase-conjugated secondary antibody for 40 min at room temperature. Band were visualized using a ChemiDoc imaging system (Bio-Rad, USA). Coomassie stain was used as a loading control. The following primary antibodies were used: Phospho (p)-AMPK Thr172 (2535S, CST), p-ACC Ser79 (07-303, Merck), p-p38MAPK Thr180/Tyr182 (9211S, CST), p-TBC1D1 Ser237 (07-2268, Merck).

Statistical analysis

Results are shown as box whiskers plots with min to max whiskers or as plots of individual data. Statistical testing was performed using t-test or one- or two-way ANOVA (repeated measurements) as appropriate. Tukey's post hoc test was performed when ANOVA revealed significance. The significance level was set at $p<0.05$.

Results:

Electroporated GLUT4-7*myc*-GFP exhibits dynamic movement and insulin-induced membrane translocation

As a first step, we validated that our *myc* antibody bound specifically to the *myc*-epitope and that it detected membrane-inserted *myc,* by incubating the antibody with non-permeabilized and permeabilized fibres with and without expression of GLUT4-7*myc*-GFP (data not shown).

Next, to test the functionality of GLUT4-7*myc*-GFP within the muscle fibres, we performed live-cell-imaging of isolated cultured FDB fibres. In accordance with previous studies describing the localization pattern of endogenous and fluorescent GLUT4 protein in skeletal muscle (Lauritzen & Schertzer, 2010; Ploug, van Deurs, Ai, Cushman, & Ralston, 1998), GLUT4-7*myc*-GFP localized to clusters of different size and was enriched in perinuclear regions (figure 1A). GLUT4-7*myc*-GFP was expressed throughout the muscle fibre in the transverse plane with a stronger signal in the superficial cytoplasmic area of the fibre (figure 1B). Worth noting, the GFP signal was lower than the Myc Alexa 568 dye signal, and Myc/GFP co-localization could therefore only be observed at the brightest Myc signal clusters. Time-lapse imaging revealed that GLUT4-7*myc*-GFP exhibited dynamic movement. While some GLUT4-7*myc*-GFP vesicles seemed static, other GLUT4-7*myc*-GFP vesicles sized <1 µm in diameter moved (figure 1C). Vesicle tracking indicated that the moving GLUT4-7*myc*-GFP vesicles were capable of travelling distances of 6-7 µm (figure 2D) on a time scale of seconds to min, in accordance with a previous study in transgenic HA-GLUT4-GFP mice (Lizunov et al., 2012). Next, to test the response of GLUT4-7myc-GFP to a physiological stimulus, kept cultured FDB fibres basal or treated them with insulin or insulin + the PI3K inhibitor wortmannin. As expected, insulin increased the *myc* signal, indicating increased

GLUT4-7myc-GFP content at the sarcolemma, compared to untreated fibres and this effect was completely blocked by wortmannin (figure 1E). Quantification indicated a ~175% increase with insulin stimulation compared to basal (ANOVA $p<0.05$, post hoc analysis $p=0.05$) (figure 1F). Surprisingly, we did not observe any discernible increase in GFP striation pattern in the insulin-treated FDB fibres *in vitro* (figure 1E). Altogether, our data demonstrated the functionality of the GLUT4-7*myc*-GFP construct in live adult muscle fibres, and its utility to quantify GLUT4 sarcolemmal accumulation.

***In vivo* exercise-stimulated GLUT4 translocation**

Exercise induces a complex array of signalling pathways (Hoffman et al., 2015) which cannot be faithfully recapitulated in reductionistic *ex vivo/in vitro* models (Sylow et al., 2017). To test the performance of the GLUT4 translocation assay *in vivo,* we subjected GLUT4-reporter electroporated mice to 15 min running at 75% (10 min) and 85% (5 min) of maximal running capacity. Running exercise induced a clear increase in *myc* signal, indicating GLUT4-7*myc*-GFP translocation to the sarcolemma (figure 2A-B). As expected, this was accompanied by increased phosphorylation of the known exercise-responsive kinasesp38 mitogen-activated protein kinase (p38 MAPK) (figure 2C&E) and AMPK (figure 2D-E). We observed no difference in exercise-stimulated 2-DG uptake between saline-injected legs and contralateral GLUT4-7*myc*-GFP-injected legs, in the subset of mice injected with [^{3}H]2-DG (figure 2F), showing that transfection of GLUT4 in a subset of muscle fibres (~20% efficiency, in the same range as seen before (Schertzer, Plant, & Lynch, 2006)) did not affect glucose uptake-responsiveness at the whole-muscle level. This demonstrated that the GLUT4-7*myc*-GFP translocation assay was suitable for detection of *in vivo* exercise-induced GLUT4 surface membrane accumulation. Of note, similar to the absent GFP-localization changes by insulin, we did not observe any discernible redistribution of GLUT4 following *in vivo* exercise (figure 2A).

***In vivo* injection of AICAR increased GLUT4 translocation**

Since AMPK activation is sufficient to increase muscle GLUT4 translocation and glucose transport (Mu, Brozinick, Valladares, Bucan, & Birnbaum, 2001), we examined whether our assay could be used for detection of AMPK-stimulated GLUT4 translocation *in vivo*. GLUT4-7*myc*-GFP *myc*-antibody detection at the sarcolemma increased robustly with AICAR

injection (figure 3A-B), again without any redistribution of the GLUT4 GFP-signal (figure 3A and figure 4A&D). As expected, AICAR injection increased Acetyl-CoA carboxylase 2 phosphorylation, a well-characterized endogenous readout of AMPK activity (Hardie & Pan, 2002) (figure 3C&F). Phosphorylation of TBC1 domain family member 1 at Ser231, an AMPK site induced by exercise in rodent and human muscle (Ser237) (Frosig, Pehmoller, Birk, Richter, & Wojtaszewski, 2010; Vichaiwong et al., 2010) was also increased by AICAR injection (figure 3D&F). p38 MAPK phosphorylation, which responds to mechanical stress but not AICAR (Jensen et al., 2014), was not changed by AICAR injection (figure 3E-F). Overall, the GLUT4-7*myc*-GFP translocation assay could thus be used to detect GLUT4 accumulation at the sarcolemma by insulin, exercise or AICAR. Despite the clear increase of GLUT4 translocation detected as sarcolemmal *myc*-signal by all 3 stimuli, we did not detect any stimulus-induced systematic change in the intracellular GLUT4 pattern detected as GFP-signal. In fact, we observed the previously described stimulus-induced GLUT4 striations as well as the described resting pattern with large (>1 μm diameter) GLUT4 membrane structures in both resting (figure 4A), insulin- (figure 4B), exercise- (figure 4C) and AICAR-stimulated (figure 4D) muscle fibres. This suggests that translocation of a minor fraction of total GLUT4 accounts for the increase in *myc*-signal.

Discussion:

The current study described a robust assay directly quantifying GLUT4 translocation, the key step for skeletal muscle glucose uptake *in vivo*. The rate-limiting step of muscle glucose uptake *in vivo* has been suggested to shift from GLUT4-dependent glucose transport to intramuscular hexokinase-dependent phosphorylation (Fueger et al., 2004; Wasserman, 2009). For this reason, we believe that measuring GLUT4 translocation in studies examining *in vivo* muscle glucose uptake is crucial to the conclusions made. Surprisingly, despite validating the performance of the assay both *in vitro* and *in vivo* using 3 different stimuli, we were unable to consistently observe the previously reported stimulus-induced decrease in large GLUT4 depots and increase in GLUT4 striation patterns, a suggestive reflection of GLUT4 translocation to t-tubules (Khan et al., 2001; Lauritzen et al., 2008; Lizunov et al., 2012; Ploug et al., 1998). Our study indicates, that GLUT4 *in toto* localization changes is not a prerequisite for increased GLUT4 presence in sarcolemma by insulin, AICAR or exercise.

Therefore, quantitative assays rather than morphological verification of GLUT4 translocation must be applied.

One previous study indicated that the t-tubules were the major site for insulin-induced GLUT4-GFP translocation (Lauritzen, Ploug, Prats, Tavare, & Galbo, 2006). Despite some inconsistency, AICAR has also been suggested to induce translocation of GLUT4 to the t-tubules (Lauritzen et al., 2010; Lemieux, Konrad, Klip, & Marette, 2003), as well as exercise (Roy & Marette, 1996). However, our assay failed to detect any significant GLUT4-7*myc*-GFP inserted into the t-tubules, except perhaps in the most superficial parts. This is clearly a limitation in this assay. Although a t-tubule staining of the HA tag in HA-GLUT4-GFP transgenic mice can be observed in collagenase-isolated FDB fibres (Lizunov et al., 2012), a previous study found a similar sarcolemmal staining as ours (Ueda et al., 2010). Since the t-tubules are narrow and tortuous, with limited diffusion capabilities (Cully et al., 2017; Shorten, McMahon, & Soboleva, 2007) and paraformaldehyde-induced cross-linking further restricts the antigenicity by limiting penetration (Eldred, Zucker, Karten, & Yazulla, 1983), it seems reasonable to assume that lack of *myc* signal in the current study was due to insufficient antibody penetration. Alternatively, the insertion of GLUT4-7*myc*-GFP in the t-tubules could be low or absent in our experimental set-up. However, given that we stimulated GLUT4 translocation both *in vitro* and *in vivo* and using both insulin, exercise and AICAR, we consider it unlikely that none of these conditions resulted in t-tubular GLUT4 translocation.

Our live imaging experiments revealed that some GLUT4-7*myc*-GFP positive vesicles exhibited dynamic movement and were capable of translocating several micrometers within a few min. Although Lauritzen and colleges did not report this type of movement, these elegant studies still suggested dynamic GLUT4-GFP movement *in situ* in muscle (Lauritzen, 2013; Lauritzen et al., 2008; Lauritzen et al., 2010; Lauritzen et al., 2006). Furthermore, it was recently reported that insulin and AICAR changed the mean velocity and mean square displacement of *myc*-GLUT4-EGFP (Hatakeyama & Kanzaki, 2017). Lizunov and colleagues reported similar long range movement as us by using total internal reflection fluorescence (TIRF) on cultured FDB fibers. Interestingly, they question the relevance of these movements

in insulin-induced GLUT4 membrane insertion (Lizunov et al., 2012). Resolving the biological function of this type of movement therefore remains an interesting research topic.

An easy to use assay quantifying endogenous GLUT4 translocation would obviously be superior to using the overexpressed GLUT4 reporter construct. GLUT4 overexpression has been reported to increase contraction-induced glucose uptake (Hansen et al., 1995), which may also be the case in our transfected fibres. Furthermore, the ultimate application would be to probe human muscle GLUT4 translocation which is not compatible with the current assay. Different approaches have been established to investigate endogenous GLUT4 translocation by both insulin and exercise/contractions in both rodent and humans (Bradley et al., 2015; Hatakeyama & Kanzaki, 2017; Klip et al., 1987; Lund, Holman, Schmitz, & Pedersen, 1993; Lund et al., 1997; Marette et al., 1992; Sylow et al., 2016; Tsuchiya et al., 2018; Wilson & Cushman, 1994). However, despite the decent positive correlation between GLUT4 translocation and glucose transport *ex vivo*, these assays in general show relatively small effect sizes on GLUT4 translocation in comparison to the amount of glucose uptake into muscle *in vivo*. Whether the effect size in our assay is enhanced due to overexpression of GLUT4 remained to be tested. However, transmission electron microscopy analysis of rat skeletal muscles revealed a ≈9-fold increase in GLUT4 in the sarcolemma following contractions (Ploug et al., 1998), indicating that this is not the case.

In conclusion, we demonstrated that electroporated GLUT4-7*myc*-GFP in mouse skeletal muscle was a robust tool to study GLUT4 dynamics and sarcolemmal accumulation by different *in vivo* stimuli including exercise and the AMPK-activator AICAR. Notably, however, the previously reported decrease in large GLUT4 vesicles and increase in striated GLUT4 pattern, respectively, by different stimuli were not observed, despite robust sarcolemmal GLUT4 insertion. This simple method could increase the frequency of GLUT4 translocation measurements in rodent loss-and gain-of-function studies of muscle glucose metabolism.

Competing interests:

None declared.

Author contributions:

Conceptualization: JRK and TEJ, Investigation: JRK, CHO, ZL, Visualization: JRK, Writing of original draft: JRK and TEJ, Revised draft: JRK with input from all authors. All authors qualify for authorship and approved the final version of the work. TEJ is accountable for all aspects of the work including the accuracy and integrity of the work.

Acknowledgements:

This study was supported by a Novo Nordisk Foundation (NNF) Excellence project grant (#15182) to TEJ, a China Scholarship Council (CSC) Ph.D. stipend to ZL and a research grant from the Danish Diabetes Academy funded by the NNF to JRK. We acknowledge the Core Facility for Integrated Microscopy, Faculty of Health and Medical Sciences, University of Copenhagen.

Reference List

Ayachi, M., Niel, R., Momken, I., Billat, V. L., & Mille-Hamard, L. (2016). Validation of a Ramp Running Protocol for Determination of the True VO2max in Mice. *Front Physiol, 7*, 372. doi:10.3389/fphys.2016.00372

Bogan, J. S., McKee, A. E., & Lodish, H. F. (2001). Insulin-responsive compartments containing GLUT4 in 3T3-L1 and CHO cells: regulation by amino acid concentrations. *Mol Cell Biol, 21*(14), 4785-4806. doi:10.1128/MCB.21.14.4785-4806.2001

Bradley, H., Shaw, C. S., Bendtsen, C., Worthington, P. L., Wilson, O. J., Strauss, J. A., . . . Wagenmakers, A. J. (2015). Visualization and quantitation of GLUT4 translocation in human skeletal muscle following glucose ingestion and exercise. *Physiol Rep, 3*(5). doi:10.14814/phy2.12375

Cline, G. W., Petersen, K. F., Krssak, M., Shen, J., Hundal, R. S., Trajanoski, Z., . . . Shulman, G. I. (1999). Impaired glucose transport as a cause of decreased insulin-stimulated muscle glycogen synthesis in type 2 diabetes. *N Engl J Med, 341*(4), 240-246. doi:10.1056/NEJM199907223410404

Close, R. I. (1972). Dynamic properties of mammalian skeletal muscles. *Physiol Rev, 52*(1), 129-197. doi:10.1152/physrev.1972.52.1.129

Cully, T. R., Murphy, R. M., Roberts, L., Raastad, T., Fassett, R. G., Coombes, J. S., . . . Launikonis, B. S. (2017). Human skeletal muscle plasmalemma alters its structure to change its Ca(2+)-handling following heavy-load resistance exercise. *Nat Commun, 8*, 14266. doi:10.1038/ncomms14266

DeFronzo, R. A., & Tripathy, D. (2009). Skeletal muscle insulin resistance is the primary defect in type 2 diabetes. *Diabetes Care, 32 Suppl 2*, S157-163. doi:10.2337/dc09-S302

Deshmukh, A. S., Murgia, M., Nagaraj, N., Treebak, J. T., Cox, J., & Mann, M. (2015). Deep proteomics of mouse skeletal muscle enables quantitation of protein isoforms, metabolic pathways, and transcription factors. *Mol Cell Proteomics, 14*(4), 841-853. doi:10.1074/mcp.M114.044222

DiFranco, M., Quinonez, M., Capote, J., & Vergara, J. (2009). DNA transfection of mammalian skeletal muscles using in vivo electroporation. *J Vis Exp*(32). doi:10.3791/1520

Eldred, W. D., Zucker, C., Karten, H. J., & Yazulla, S. (1983). Comparison of fixation and penetration enhancement techniques for use in ultrastructural immunocytochemistry. *J Histochem Cytochem, 31*(2), 285-292. doi:10.1177/31.2.6339606

Frosig, C., Pehmoller, C., Birk, J. B., Richter, E. A., & Wojtaszewski, J. F. (2010). Exercise-induced TBC1D1 Ser237 phosphorylation and 14-3-3 protein binding capacity in human skeletal muscle. *J Physiol, 588*(Pt 22), 4539-4548. doi:10.1113/jphysiol.2010.194811

Fueger, P. T., Hess, H. S., Posey, K. A., Bracy, D. P., Pencek, R. R., Charron, M. J., & Wasserman, D. H. (2004). Control of exercise-stimulated muscle glucose uptake by GLUT4 is dependent on glucose phosphorylation capacity in the conscious mouse. *J Biol Chem, 279*(49), 50956-50961. doi:10.1074/jbc.M408312200

Goodpaster, B. H., Bertoldo, A., Ng, J. M., Azuma, K., Pencek, R. R., Kelley, C., . . . Kelley, D. E. (2014). Interactions among glucose delivery, transport, and phosphorylation that underlie skeletal muscle insulin resistance in obesity and type 2 Diabetes: studies with dynamic PET imaging. *Diabetes, 63*(3), 1058-1068. doi:10.2337/db13-1249

Hansen, P. A., Gulve, E. A., Marshall, B. A., Gao, J., Pessin, J. E., Holloszy, J. O., & Mueckler, M. (1995). Skeletal muscle glucose transport and metabolism are enhanced in transgenic mice overexpressing the Glut4 glucose transporter. *J Biol Chem, 270*(4), 1679-1684.

Hansen, P. A., Nolte, L. A., Chen, M. M., & Holloszy, J. O. (1998). Increased GLUT-4 translocation mediates enhanced insulin sensitivity of muscle glucose transport after exercise. *J Appl Physiol (1985), 85*(4), 1218-1222. doi:10.1152/jappl.1998.85.4.1218

Hardie, D. G., & Pan, D. A. (2002). Regulation of fatty acid synthesis and oxidation by the AMP-activated protein kinase. *Biochem Soc Trans, 30*(Pt 6), 1064-1070. doi:10.1042/

Hatakeyama, H., & Kanzaki, M. (2017). Heterotypic endosomal fusion as an initial trigger for insulin-induced glucose transporter 4 (GLUT4) translocation in skeletal muscle. *J Physiol, 595*(16), 5603-5621. doi:10.1113/JP273985

Hoffman, N. J., Parker, B. L., Chaudhuri, R., Fisher-Wellman, K. H., Kleinert, M., Humphrey, S. J., . . . James, D. E. (2015). Global Phosphoproteomic Analysis of Human Skeletal Muscle Reveals a Network of Exercise-Regulated Kinases and AMPK Substrates. *Cell Metab, 22*(5), 922-935. doi:10.1016/j.cmet.2015.09.001

Holman, G. D., Kozka, I. J., Clark, A. E., Flower, C. J., Saltis, J., Habberfield, A. D., . . . Cushman, S. W. (1990). Cell surface labeling of glucose transporter isoform GLUT4 by bis-mannose photolabel. Correlation with stimulation of glucose transport in rat adipose cells by insulin and phorbol ester. *J Biol Chem, 265*(30), 18172-18179.

Jaldin-Fincati, J. R., Pavarotti, M., Frendo-Cumbo, S., Bilan, P. J., & Klip, A. (2017). Update on GLUT4 Vesicle Traffic: A Cornerstone of Insulin Action. *Trends Endocrinol Metab, 28*(8), 597-611. doi:10.1016/j.tem.2017.05.002

Jensen, T. E., Ross, F. A., Kleinert, M., Sylow, L., Knudsen, J. R., Gowans, G. J., . . . Richter, E. A. (2015). PT-1 selectively activates AMPK-gamma1 complexes in mouse skeletal muscle, but activates all three gamma subunit complexes in cultured human cells by inhibiting the respiratory chain. *Biochem J*. doi:10.1042/BJ20141142

Jensen, T. E., Sylow, L., Rose, A. J., Madsen, A. B., Angin, Y., Maarbjerg, S. J., & Richter, E. A. (2014). Contraction-stimulated glucose transport in muscle is controlled by AMPK and mechanical stress but not sarcoplasmatic reticulum Ca(2+) release. *Mol Metab, 3*(7), 742-753. doi:10.1016/j.molmet.2014.07.005

Kanai, F., Nishioka, Y., Hayashi, H., Kamohara, S., Todaka, M., & Ebina, Y. (1993). Direct demonstration of insulin-induced GLUT4 translocation to the surface of intact cells by insertion of a c-myc epitope into an exofacial GLUT4 domain. *J Biol Chem, 268*(19), 14523-14526.

Khan, A. H., Thurmond, D. C., Yang, C., Ceresa, B. P., Sigmund, C. D., & Pessin, J. E. (2001). Munc18c regulates insulin-stimulated glut4 translocation to the transverse tubules in skeletal muscle. *J Biol Chem, 276*(6), 4063-4069. doi:10.1074/jbc.M007419200

Klip, A., Ramlal, T., Young, D. A., & Holloszy, J. O. (1987). Insulin-induced translocation of glucose transporters in rat hindlimb muscles. *FEBS Lett, 224*(1), 224-230.

Kristiansen, S., Hargreaves, M., & Richter, E. A. (1996). Exercise-induced increase in glucose transport, GLUT-4, and VAMP-2 in plasma membrane from human muscle. *Am J Physiol, 270*(1 Pt 1), E197-201.

Lauritzen, H. P. (2013). Insulin- and contraction-induced glucose transporter 4 traffic in muscle: insights from a novel imaging approach. *Exerc Sport Sci Rev, 41*(2), 77-86. doi:10.1097/JES.0b013e318275574c

Lauritzen, H. P., Galbo, H., Brandauer, J., Goodyear, L. J., & Ploug, T. (2008). Large GLUT4 vesicles are stationary while locally and reversibly depleted during transient insulin stimulation of skeletal muscle of living mice: imaging analysis of GLUT4-enhanced green fluorescent protein vesicle dynamics. *Diabetes, 57*(2), 315-324. doi:10.2337/db06-1578

Lauritzen, H. P., Galbo, H., Toyoda, T., & Goodyear, L. J. (2010). Kinetics of contraction-induced GLUT4 translocation in skeletal muscle fibers from living mice. *Diabetes, 59*(9), 2134-2144. doi:10.2337/db10-0233

Lauritzen, H. P., Ploug, T., Prats, C., Tavare, J. M., & Galbo, H. (2006). Imaging of insulin signaling in skeletal muscle of living mice shows major role of T-tubules. *Diabetes, 55*(5), 1300-1306.

Lauritzen, H. P., & Schertzer, J. D. (2010). Measuring GLUT4 translocation in mature muscle fibers. *Am J Physiol Endocrinol Metab, 299*(2), E169-179. doi:10.1152/ajpendo.00066.2010

Lemieux, K., Konrad, D., Klip, A., & Marette, A. (2003). The AMP-activated protein kinase activator AICAR does not induce GLUT4 translocation to transverse tubules but stimulates glucose uptake and p38 mitogen-activated protein kinases alpha and beta in skeletal muscle. *FASEB J, 17*(12), 1658-1665. doi:10.1096/fj.02-1125com

Leto, D., & Saltiel, A. R. (2012). Regulation of glucose transport by insulin: traffic control of GLUT4. *Nat Rev Mol Cell Biol, 13*(6), 383-396. doi:10.1038/nrm3351

Lizunov, V. A., Stenkula, K. G., Lisinski, I., Gavrilova, O., Yver, D. R., Chadt, A., . . . Cushman, S. W. (2012). Insulin stimulates fusion, but not tethering, of GLUT4 vesicles in skeletal muscle of HA-GLUT4-GFP transgenic mice. *Am J Physiol Endocrinol Metab, 302*(8), E950-960. doi:10.1152/ajpendo.00466.2011

Lund, S., Holman, G. D., Schmitz, O., & Pedersen, O. (1993). Glut 4 content in the plasma membrane of rat skeletal muscle: comparative studies of the subcellular fractionation method and the exofacial photolabelling technique using ATB-BMPA. *FEBS Lett, 330*(3), 312-318.

Lund, S., Holman, G. D., Schmitz, O., & Pedersen, O. (1995). Contraction stimulates translocation of glucose transporter GLUT4 in skeletal muscle through a mechanism distinct from that of insulin. *Proc Natl Acad Sci U S A, 92*(13), 5817-5821.

Lund, S., Holman, G. D., Zierath, J. R., Rincon, J., Nolte, L. A., Clark, A. E., . . . Wallberg-Henriksson, H. (1997). Effect of insulin on GLUT4 cell surface content and turnover rate in human skeletal muscle as measured by the exofacial bis-mannose photolabeling technique. *Diabetes, 46*(12), 1965-1969.

Madsen, A. B., Knudsen, J. R., Henriquez-Olguin, C., Angin, Y., Zaal, K. J., Sylow, L., . . . Jensen, T. E. (2018). beta-Actin shows limited mobility and is required only for supraphysiological insulin-stimulated glucose transport in young adult soleus muscle. *Am J Physiol Endocrinol Metab, 315*(1), E110-E125. doi:10.1152/ajpendo.00392.2017

Marette, A., Burdett, E., Douen, A., Vranic, M., & Klip, A. (1992). Insulin induces the translocation of GLUT4 from a unique intracellular organelle to transverse tubules in rat skeletal muscle. *Diabetes, 41*(12), 1562-1569.

Martin, I. K., Katz, A., & Wahren, J. (1995). Splanchnic and muscle metabolism during exercise in NIDDM patients. *Am J Physiol, 269*(3 Pt 1), E583-590.

Mauro, A., & Adams, W. R. (1961). The structure of the sarcolemma of the frog skeletal muscle fiber. *J Biophys Biochem Cytol, 10(4)Suppl*, 177-185.

Mu, J., Brozinick, J. T., Jr., Valladares, O., Bucan, M., & Birnbaum, M. J. (2001). A role for AMP-activated protein kinase in contraction- and hypoxia-regulated glucose transport in skeletal muscle. *Mol Cell, 7*(5), 1085-1094.

Ploug, T., van Deurs, B., Ai, H., Cushman, S. W., & Ralston, E. (1998). Analysis of GLUT4 distribution in whole skeletal muscle fibers: identification of distinct storage compartments that are recruited by insulin and muscle contractions. *J Cell Biol, 142*(6), 1429-1446.

Ploug, T., Wojtaszewski, J., Kristiansen, S., Hespel, P., Galbo, H., & Richter, E. A. (1993). Glucose transport and transporters in muscle giant vesicles: differential effects of insulin and contractions. *Am J Physiol, 264*(2 Pt 1), E270-278. doi:10.1152/ajpendo.1993.264.2.E270

Richter, E. A., & Hargreaves, M. (2013). Exercise, GLUT4, and skeletal muscle glucose uptake. *Physiol Rev, 93*(3), 993-1017. doi:10.1152/physrev.00038.2012

Rose, A. J., Jeppesen, J., Kiens, B., & Richter, E. A. (2009). Effects of contraction on localization of GLUT4 and v-SNARE isoforms in rat skeletal muscle. *Am J Physiol Regul Integr Comp Physiol, 297*(5), R1228-1237. doi:10.1152/ajpregu.00258.2009

Roy, D., & Marette, A. (1996). Exercise induces the translocation of GLUT4 to transverse tubules from an intracellular pool in rat skeletal muscle. *Biochem Biophys Res Commun, 223*(1), 147-152. doi:10.1006/bbrc.1996.0860

Schermelleh, L., Heintzmann, R., & Leonhardt, H. (2010). A guide to super-resolution fluorescence microscopy. *J Cell Biol, 190*(2), 165-175. doi:10.1083/jcb.201002018

Schertzer, J. D., Antonescu, C. N., Bilan, P. J., Jain, S., Huang, X., Liu, Z., . . . Klip, A. (2009). A transgenic mouse model to study glucose transporter 4myc regulation in skeletal muscle. *Endocrinology, 150*(4), 1935-1940. doi:10.1210/en.2008-1372

Schertzer, J. D., Plant, D. R., & Lynch, G. S. (2006). Optimizing plasmid-based gene transfer for investigating skeletal muscle structure and function. *Mol Ther, 13*(4), 795-803. doi:10.1016/j.ymthe.2005.09.019

Shepherd, P. R., & Kahn, B. B. (1999). Glucose transporters and insulin action--implications for insulin resistance and diabetes mellitus. *N Engl J Med, 341*(4), 248-257. doi:10.1056/NEJM199907223410406

Shorten, P. R., McMahon, C. D., & Soboleva, T. K. (2007). Insulin transport within skeletal muscle transverse tubule networks. *Biophys J, 93*(9), 3001-3007. doi:10.1529/biophysj.107.107888

Sylow, L., Moller, L. L. V., Kleinert, M., D'Hulst, G., De Groote, E., Schjerling, P., . . . Richter, E. A. (2017). Rac1 and AMPK Account for the Majority of Muscle Glucose Uptake Stimulated by Ex Vivo Contraction but Not In Vivo Exercise. *Diabetes, 66*(6), 1548-1559. doi:10.2337/db16-1138

Sylow, L., Nielsen, I. L., Kleinert, M., Moller, L. L., Ploug, T., Schjerling, P., . . . Richter, E. A. (2016). Rac1 governs exercise-stimulated glucose uptake in skeletal muscle through regulation of GLUT4 translocation in mice. *J Physiol, 594*(17), 4997-5008. doi:10.1113/JP272039

Tsuchiya, M., Sekiai, S., Hatakeyama, H., Koide, M., Chaweewannakorn, C., Yaoita, F., . . . Kanzaki, M. (2018). Neutrophils Provide a Favorable IL-1-Mediated Immunometabolic Niche that Primes GLUT4 Translocation and Performance in Skeletal Muscles. *Cell Rep, 23*(8), 2354-2364. doi:10.1016/j.celrep.2018.04.067

Ueda, S., Kitazawa, S., Ishida, K., Nishikawa, Y., Matsui, M., Matsumoto, H., . . . Satoh, T. (2010). Crucial role of the small GTPase Rac1 in insulin-stimulated translocation of glucose transporter 4 to the mouse skeletal muscle sarcolemma. *FASEB J, 24*(7), 2254-2261. doi:10.1096/fj.09-137380

Vichaiwong, K., Purohit, S., An, D., Toyoda, T., Jessen, N., Hirshman, M. F., & Goodyear, L. J. (2010). Contraction regulates site-specific phosphorylation of TBC1D1 in skeletal muscle. *Biochem J, 431*(2), 311-320. doi:10.1042/BJ20101100

Warram, J. H., Martin, B. C., Krolewski, A. S., Soeldner, J. S., & Kahn, C. R. (1990). Slow glucose removal rate and hyperinsulinemia precede the development of type II diabetes in the offspring of diabetic parents. *Ann Intern Med, 113*(12), 909-915.

Wasserman, D. H. (2009). Four grams of glucose. *Am J Physiol Endocrinol Metab, 296*(1), E11-21. doi:10.1152/ajpendo.90563.2008

Wilson, C. M., & Cushman, S. W. (1994). Insulin stimulation of glucose transport activity in rat skeletal muscle: increase in cell surface GLUT4 as assessed by photolabelling. *Biochem J, 299 (Pt 3)*, 755-759.

Zisman, A., Peroni, O. D., Abel, E. D., Michael, M. D., Mauvais-Jarvis, F., Lowell, B. B., . . . Kahn, B. B. (2000). Targeted disruption of the glucose transporter 4 selectively in muscle causes insulin resistance and glucose intolerance. *Nat Med, 6*(8), 924-928. doi:10.1038/78693

Figure legends:

Figure 1: GLUT4-7*myc*-GFP localized to larger vesicles and in perinuclear regions, exhibited dynamic movement and responded to insulin. A) GFP signal of live flexor digitorum brevis (FDB) muscle fibre expressing GLUT4-7*myc*-GFP. Arrows mark perinuclear regions, arrowheads mark intracellular vesicles of varying size. B) Z-axis profile plot of GFP signal throughout the transverse plane of a live FDB fibre. Red arrows marks increased fluorescent intensity in the superficial regions of the fibre. C) Live imaging montage of GFP movement in FDB fibre. Yellow arrowheads with circles mark a moving GFP-containing vesicle. Colored dots mark tracking of 6 different GFP-containing vesicles over time. D) Migration scheme of 150 sec tracking of GFP containing vesicles in C (location A) and another migration scheme from different region (location B). E) Representative images of GFP signal (lower panels) and *myc* signal (upper panels) of cultured FDB fibres expressing GLUT4-7m*yc*-GFP incubated in the basal state (left), stimulated with 60 nM insulin (INS, middle) or stimulated with 60 nM insulin and 500 nM wortmanin (INS+Wort., right). F) Quantification of GLUT4 translocation measured as *myc*/GFP signal ratio. A-D are representative of 3 independent experiments. For E&F 9,4 and 3basal, INS and INS+Wort. treated fibres from two different mice were analysed. *p=0.05 different from basal. Scale bar = 5 µm (A,C&D) or 20 µm (E).

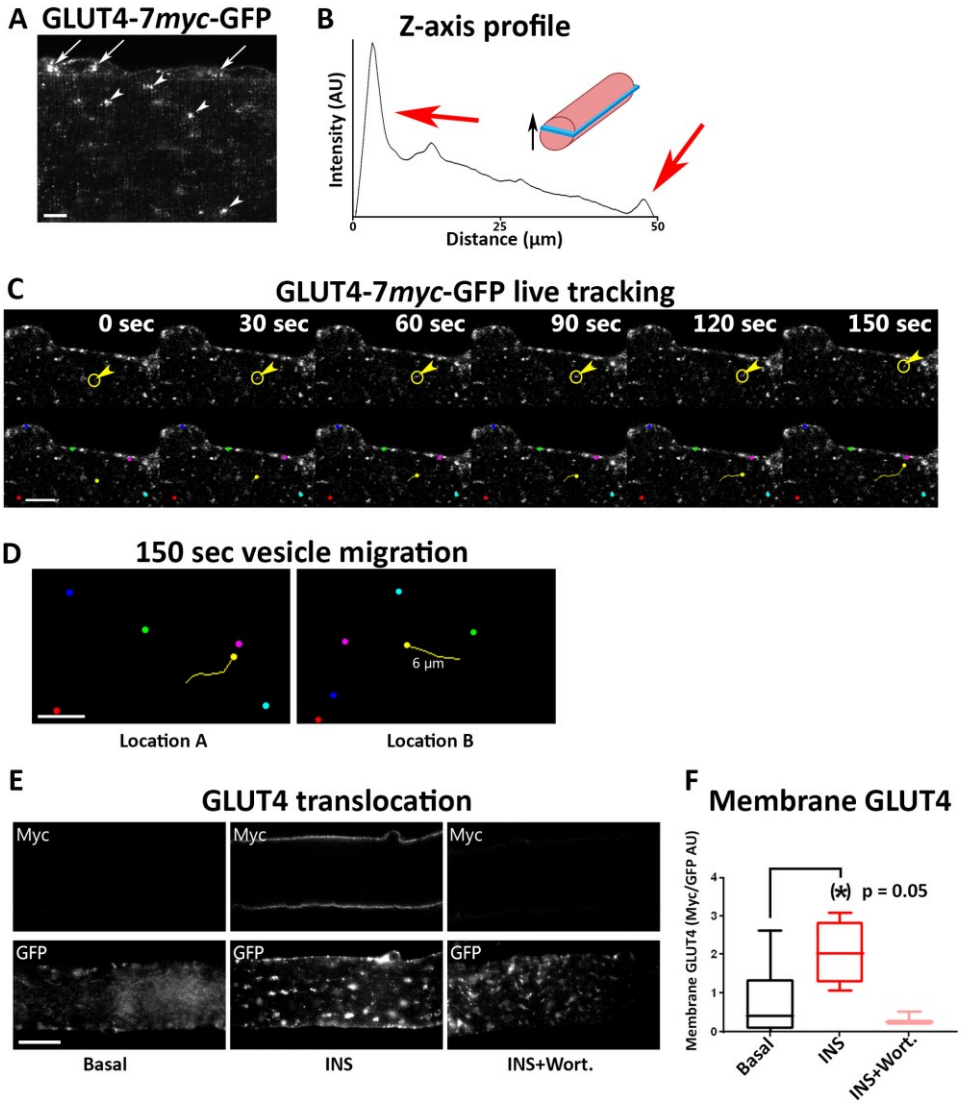

Figure 2: *In vivo* exercise stimulated GLUT4 translocation in tibialis anterior muscle. A) Representative images of GFP signal (lower panels) and *myc* signal (upper panels) of tibialis anterior (TA) muscle fibres from mice subjected to running exercise. Mice ran for 15 minutes (10 min at 75% and 5 min at 85% of max running capacity). B) Quantification of GLUT4 translocation measured as *myc*/GFP ratio. n = 32 and 39 resting and exercised fibres in each condition respectively, from 3 mice in 3 independent experiments were analysed. C) Phosphorylation of p38 Mitogen-activated protein kinase (MAPK) Thr180/Tyr182 and D) phosphorylation of AMP-activated protein kinase (AMPK) Thr172 in soleus muscles from mice subjected to same running exercise bout as in A. E) Representative western blot images from C&D (n=4). F) 2-deoxyglucose transport into TA muscles from mice subjected to gene transfer procedure after injection of saline in one leg and GLUT4-7*myc*-GFP in the contralateral leg. Mice (n=4-6) ran as described in A. (*) p=0.07 , **/***p<0.01/0.001 effect of exercise. Scale bar = 20 µm.

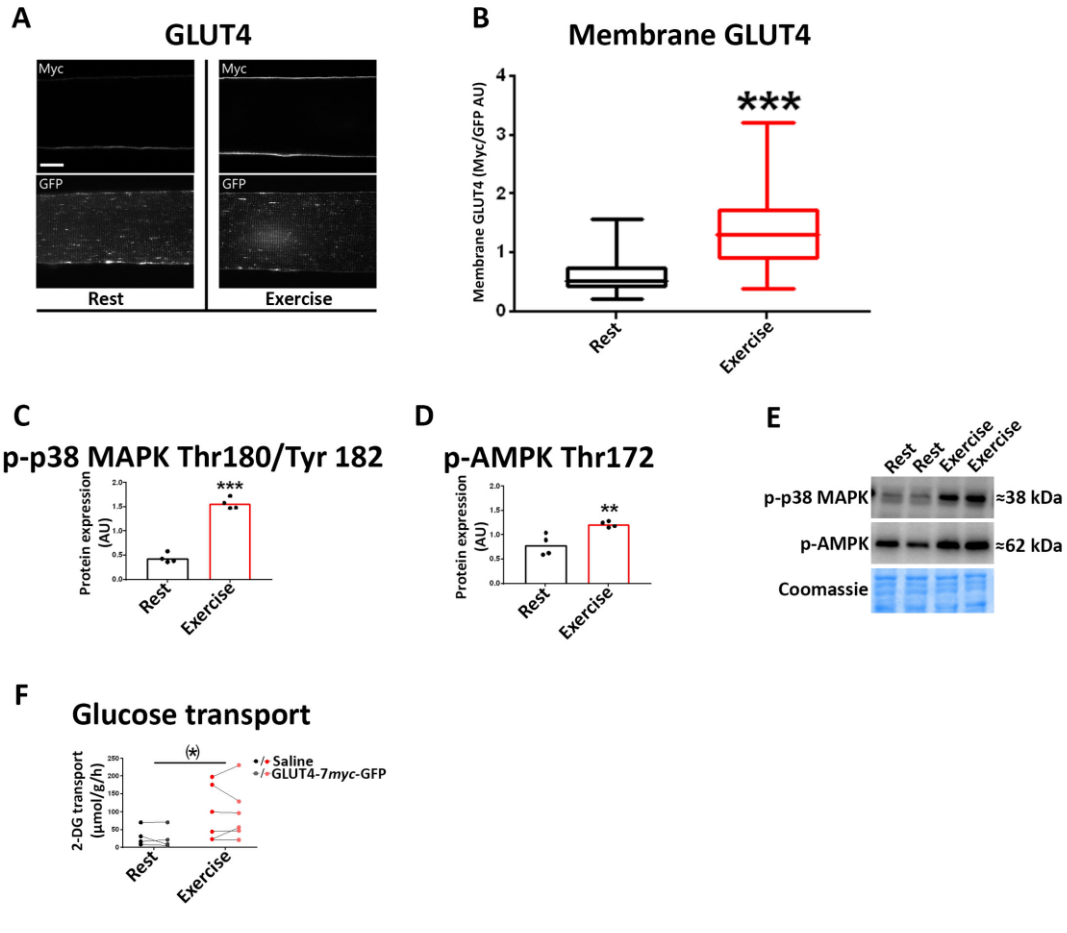

Figure 3: Intramuscular AICAR injection stimulated AMPK and GLUT4 translocation. A) Phosphorylation of Acetyl-CoA carboxylase (ACC) ser212, B) TBC1 domain family member 1 (TBC1D1) ser231 and C) p38 Mitogen-activated protein kinase (MAPK) Thr180/Tyr182 in TA muscles injected with AICAR or saline (n=12). D) Representative western blot images from A,B&C. E) Representative images of GFP signal (lower panels) and *myc* signal (upper panels) of TA muscle fibres from mice intramuscularly injected with saline or AICAR. F) Quantification of GLUT4 translocation measured as *myc*/GFP signal ratio. 38 and 42 saline or AICAR treated fibres from 4 different muscles in each condition were analysed. ***p<0.001 effect of AICAR. Scale bar = 20 µm.

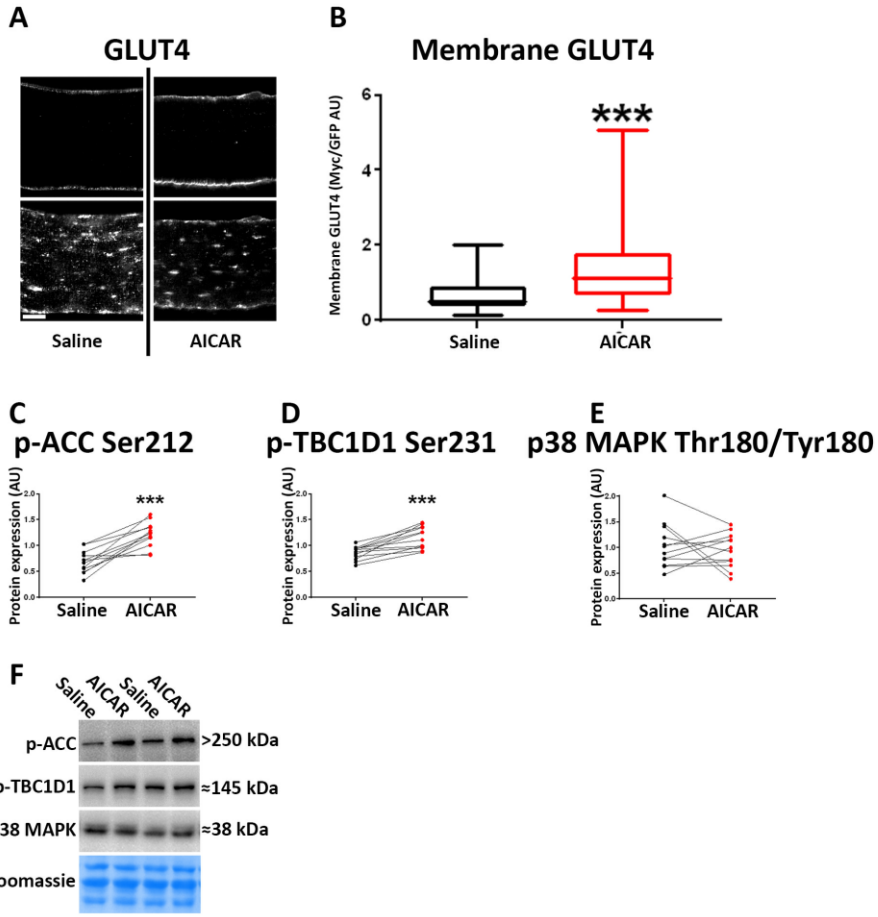

Figure 4: GLUT4-7*myc*-GFP distributed in several localization patterns without discernible changes induced by any stimuli. A) GFP signal in TA muscle fibres expressing GLUT4-7*myc*-GFP from mice kept at rest. B) Same as in A in mice stimulated with 0.5 U insulin/kg body weight 30 min prior to fixation of muscle. C) Same as in A in mice performing running exercise, as described in the methods section. D) Same as in A but from mice stimulated with AICAR, as described in the methods sections. Insulin (INS), exercise (EXER) and AICAR (AIC). Scale bar = 20 μm.